Published in final edited form as:
AJR Am J Roentgenol. 2009 August ; 193(2): 304–313. doi:10.2214/AJR.09.2869.

Imaging of Tumor Angiogenesis: Functional or Targeted?

Baris Turkbey, **Hisataka Kobayashi**, **Mikako Ogawa**, **Marcelino Bernardo**, and **Peter L. Choyke**
Molecular Imaging Program, National Cancer Institute, National Institutes of Health, 10 Center Dr., MSC 1182, Bldg. 10, Rm. 1B40, Bethesda, MD 20892-1088

Abstract

OBJECTIVE—Angiogenesis—the growth of new vessels—is both a normal physiologic response and a critical step in many pathologic processes, particularly cancer. Imaging has long relied on the different enhancement characteristics of cancer compared with normal tissue; the information generated is often primarily morphologic and qualitative. However, more quantitative methods based on functional and targeted imaging have recently emerged.

CONCLUSION—In this article, we review both functional and targeted imaging techniques for assessing tumor angiogenesis.

Keywords

angiogenesis; functional imaging; targeted imaging; tumor angiogenesis

Angiogenesis—the growth of new vessels—is both a normal physiologic response and a critical step in many pathologic processes, particularly cancer. Tumors must generate their own blood supply once they have grown to a diameter of 2–3 mm and can no longer subsist on diffusion of nutrients from the existing host microvasculature [1]. Tumors secrete a number of growth factors and proteolytic enzymes into the interstitium that act on endothelial cells and basement membranes to remodel existing vessels and stimulate the release of endothelial progenitor stem cells from the bone marrow to form new vessels [2]. However, unlike highly controlled physiologic angiogenesis, tumor angiogenesis results in chaotic, inefficient, and permeable vessels that are distinct from the normal vasculature (Fig. 1). Because such vessels are accessible to the systemic vasculature and are unique vital components of the tumor's growth strategy, they make excellent targets for molecular therapies. Thus, a variety of antibody-based and small molecule inhibitors of angiogenesis have emerged. These antiangiogenesis therapies have led to an increased interest in imaging as a means of monitoring therapeutic effect. These new therapies are expensive and do not provide benefit in all cases. Therefore, noninvasive imaging biomarkers that assess angiogenic response early in the course of therapy could be useful in directing patients to remain on therapy or to quickly move to other, more effective therapies for their tumor.

Although imagers have long relied on the different enhancement characteristics of cancer compared with normal tissue, the information generated is often primarily morphologic (e.g., size) and qualitative (e.g., hyperenhancing vs hypoenhancing). However, more quantitative methods based on functional and targeted imaging have recently emerged. Herein, we review both functional and targeted imaging techniques for assessing tumor angiogenesis.

Address correspondence to P. L. Choyke (pchoyke@mail.nih.gov).

Functional Imaging Techniques

Ultrasound

Ultrasound, with the combined use of gray-scale and color and power Doppler ultrasound modes, can depict the patency and flow dynamics of larger vessels in tumors; these vessels are generally larger than the diameter of angiogenic capillaries, which are typically less than 500 μm in diameter. Thus, Doppler ultrasound more likely measures flow and flow resistance in the native vasculature or, as in the case in which additional mature vessels have been recruited to the tumor, vasculogenesis. Analysis of spectral waveforms, which measure blood velocity, direction, and downstream resistance, has met with variable success for differentiating benign and malignant lesions (Fig. 2). For instance, the resistive index (RI) can reflect diastolic vascular resistance in a tumor bed. In peripheral tumor vessels, low vascular resistance is related to the lack of vasomotor control and arteriovenous shunting, whereas in more central vessels, high vascular resistance related to high oncotic interstitial pressures is seen. Thus, the heterogeneous nature of tumor vascularity may lead to the detection of both high and low RI values in the same lesion; moreover, there can be significant overlap of RIs between benign and malignant lesions [3]. RI measurements have been reported to correlate with microvessel density (MVD) in breast and ovarian cancer, but the relationship is indirect because the microvessels are significantly below the spatial resolution of ultrasound [4–6]. Contrast-enhanced ultrasound with microbubbles allows the depiction of smaller vessels and the assessment of response to antiangiogenesis treatment in several tumor types [7–14]. However, because of limitations in spatial resolution, operator dependence, the short time window available for imaging, and the limited field of view, microbubble ultrasound is used in the assessment of angiogenesis in only a few centers worldwide.

CT Perfusion

CT perfusion or dynamic contrast-enhanced CT (DCE-CT) is the acquisition of serial images through the same volume over time after the administration of a bolus of iodinated contrast media. Because of the excellent linearity between tissue attenuation and iodine concentration, DCE-CT is amenable to analysis that allows estimates of blood flow and blood volume in tumors. This technique was first used in the evaluation of acute stroke patients, but it has also been reported to be useful in the detection of tumor angiogenesis and in assessing response to antiangiogenesis treatment [15–20] (Fig. 3). Tissue enhancement curves can be mathematically fit to compartmental or deconvolution models, and quantitative parameters such as blood volume, blood flow, mean transit time, and capillary permeability surface can be obtained [21]. Ma et al. [15] evaluated the relationship between CT perfusion findings, tumor angiogenesis, and vascular endothelial growth factor (VEGF) expression in patients with benign and malignant pulmonary nodules; they assessed the nodules using several descriptive parameters such as peak height enhancement and peak height enhancement ratio of lesion to aorta, and they calculated parameters such as blood flow, blood volume, and capillary permeability surface obtained on perfusion maps. They correlated the CT perfusion parameters with tumor angiogenesis, MVD, and VEGF expression. Li et al. [18] investigated the correlation between MVD and CT perfusion findings in 37 patients with colorectal cancer using time– density curves from CT perfusion. They concluded that CT perfusion imaging can be accurate in the assessment of angiogenesis in colorectal carcinoma. Despite its irrefutable benefits, CT perfusion has the major drawback of radiation exposure, about which public awareness has increased. This limits the number of such studies permissible in the course of a clinical trial; however, implementation of low-dose scanning protocols may allow more the widespread and frequent use of this technique.

Dynamic Contrast-Enhanced MRI

Dynamic contrast-enhanced MRI (DCEMRI) is performed by applying fast T1- weighted 3D MRI sequences before, during, and after the IV injection of a low-molecular- weight gadolinium chelate [22]. On DCE-MRI, tumors classically show rapid and intense enhancement followed by deenhancement, which is faster than normal background tissue. However, there is considerable variation in this pattern among tumor types and significant heterogeneity within individual tumors. Although these properties can be readily detected in larger lesions, they are often more difficult to visualize in smaller lesions.

DCE-MR images can be evaluated using a variety of different analytic techniques. With descriptive analysis, the shape of the signal intensity-versus-time curve can be described by its onset time relative to injection, slope of the initial enhancement, time to peak, slope of the washout curve, and area under the curve (AUC). Descriptive analysis is relatively easy to perform but is dependent on the precise scanning conditions, timing of injection, status of the patient, and a host of other variables, and is therefore difficult to replicate. Moreover, the data are strictly descriptive, without inherent physiologic meaning. Another analytic approach involves quantifying the gadolinium concentration using a T1 map and fitting the gadolinium concentration curve to a kinetic model. In MRI, there is no linear relationship between the concentration of gadolinium and tissue signal intensity as there is with CT between the concentration of iodine and tissue Hounsfield units. However, T1 maps can introduce additional errors if the scanners are not carefully calibrated. A pharmacokinetic model is used to fit the enhancement curves that enable the calculation of vascular permeability constants, K^{trans} (transendothelial transport of contrast medium from vascular compartment to the tumor interstitium), k_{ep} (reverse transport parameter of contrast medium back into the vascular space), fpV (plasma volume fraction compared with whole-tissue volume), and V_e (extravascular, extracellular space fraction of the tumor for describing tumor and tissue permeability) [23]. The terms “wash in” and “washout” are to be avoided because they are overly simplistic descriptors of what these parameters represent. The kinetic parameters are usually higher in tumors than in surrounding healthy tissue, but they can decrease significantly after antiangiogenesis treatment.

A central flaw of the current practice of DCE-MRI is that there is poor adherence to the standard nomenclature, and acquisition methods and pharmacokinetic models vary widely. Thus, comparing studies from different institutions is difficult. One controversy that has not yet been resolved is whether an arterial input function should be included in the analysis to ensure that the parameters are not unduly influenced by the contrast injection rate or the hemodynamic status of the patient. In theory, the arterial input function optimizes the quantitative analysis by measuring the signal from an artery near the tumor; however, artifacts from flowing blood in large adjacent vessels and a nonuniform radiofrequency excitation field can introduce errors into the calculation if not properly handled, thereby reducing the reliability of DCE-MRI rather than improving it. Moreover, the adjacent large vessel may not reflect the actual arterial input to the tumor. After defining an arterial input function and establishing the unenhanced T1 map, two-compartment DCE-MRI analysis can be performed with dedicated analysis tools. In addition to providing quantitative parameters (K^{trans}, k_{ep}, V_e, fpV), color-coded tissue parametric maps reflecting these constants can also be generated to assist in the diagnostic display of the data [22]. A consensus on imaging protocol and analysis tools is needed to improve the repeatability, reproducibility, and standardization of DCE-MRI.

DCE-MRI has been used as a biomarker for monitoring response to conventional chemotherapy and antiangiogenesis therapy, as well as to radiotherapy and embolotherapy for various cancer types such as breast, prostate, colon, and gynecologic malignancies [24–35] (Figs. 4 and 5). Thukral et al. [32] compared three DCE-MRI analytic methods

(heuristic, Brix, and general kinetic models) to determine the parameter or combination of parameters most strongly associated with changes in tumor microvasculature during treatment with bevacizumab alone and with bevacizumab plus chemotherapy in patients with inflammatory or locally advanced breast cancer; they reported K^{trans}, k_{ep}, and the integrated area under the gadolinium concentration curve to have the strongest association with early physiologic response to bevacizumab. Ocak et al. [34] reported improvement of the specificity of MRI at 3 T for prostate cancer by also performing DCE-MRI and by using pharmacokinetic parameters, particularly K^{trans} and k_{ep}, for analysis.

DCE-MRI is currently performed with clinically approved low-molecular-weight gadolinium chelates, which readily pass through the endothelium of angiogenic vessels. Because inflammatory tissue and neoplastic tissue have leaky vessels, enhancement is nonspecific; however, neoplastic vessels commonly have larger vascular pores than do inflammatory vessels. Thus, macromolecular MR contrast agents (e.g., ultra-small paramagnetic iron oxides, gadolinium albumin, gadolinium liposomes, gadolinium dendrimers, and gadolinium viral particles) may be more selective for tumor-induced angiogenesis than are low-molecular-weight contrast agents (Fig. 6). Macromolecular contrast agents generally result in lower permeability constants and lower effective vascular fractions because of their reduced leakiness. Because they leak less, they result in less enhancement than low-molecular-weight agents; however, this is partly overcome by the improved relaxivities of macromolecular agents. Such agents are not widely available for clinical use and there is a lack of clinical experience with them; most of the experience is limited to animal tumor models [36, 37].

Implementation of DCE-MRI into clinical practice poses several challenges. DCE-MRI is limited in organs with physiologic motion such as the lungs and liver; breath-holding, deformation registration, or navigator pulses may be needed to correct motion errors [38, 39]. Importantly, there is no adequate validation methodology for DCE-MRI, specifically for assessing the response to antiangiogenesis treatment because most tissue markers are static and simply reflect the density of vessels, not their functional abnormality. Finally, DCE-MRI may not be feasible for some patient groups, especially individuals with kidney failure (because of the risk of nephrogenic systemic fibrosis), those with implanted metallic devices (cardiac pacemakers, prosthetic valves, intracranial aneurysmal clips, shrapnel injury), and those with severe claustrophobia.

Functional PET

PET can be thought of as either a functional imaging technique or a targeted imaging technique. For functional PET, ^{15}O-labeled radiotracers such as $H_2\,^{15}O$ and $C^{15}O$, have been used to quantify tumor angiogenesis [40–42]. For instance, $H_2\,^{15}O$ (labeled water), when injected as a bolus, can be used to measure blood flow using a Patlak approach. $C^{15}O$ (labeled carbon monoxide) immediately binds to RBCs in vivo, allowing assessment of blood volume; another alternative is to label the molecule with ^{11}C, which has an ~ 20-minute half-life versus ~ 2 minutes for ^{15}O. However, the short half-life of ^{15}O and ^{11}C requires on-site synthesis in cyclotrons and immediate radiochemistry, facilities that only a few institutions possess [43]. Fluorine-18, with its 90-minute half-life, is a better overall PET radiotracer and can be produced offsite; ^{18}F-FDG is the most widely used radiotracer in PET and reflects the glucose metabolism of tumor cells. However, the links between FDG uptake and angiogenesis, as measured by MVD, of tumor lesions are variable and inconsistent [44–48]. Therefore, the more promising applications of PET are with molecularly targeted probes, as will be discussed next.

Molecular Imaging of Tumor Angiogenesis: A Targeted Technique

Molecules Selectively Expressed on Neoangiogenic Vessels: Targets

Because new molecular therapies are directed at specific targets, it follows that molecular imaging, directed at the same or related targets, might be useful in predicting drug response. A targeted approach relies on binding of labeled molecules to highly expressed markers on the endothelium of tumor vasculature. Among the molecules that are potential targets for imaging are VEGF and its receptors (VEGF receptor types 1, 2, and 3), integrins, and matrix metalloproteinases (MMPs).

The VEGF/VEGF receptor axis is one of the most extensively studied angiogenesis-related signaling pathways. VEGF receptor-1 is important for physiologic and developmental angiogenesis, whereas VEGF receptor-2 is vital for the mitogenic, angiogenic, and permeability- enhancing effects of VEGF. Upregulation and overexpression of VEGF are poor prognostic indicators for several cancer types [49]. Inhibitors of the VEGF/VEGF receptor pathway have been proven to be effective in human trials [50, 51], and overexpression of one or more targets in the VEGR/VEGF receptor pathway have been the basis for several molecular imaging agents [52–59] (Table 1).

Integrins are cell adhesion molecules, which are highly expressed on the surface of endothelial cells [60]. They mediate endothelial cell migration and survival during tumor angiogenesis and can also be expressed on tumor cells. Among several types of integrins, the $\alpha_v\beta_3$ integrin is often significantly up-regulated in activated endothelial cells during angiogenesis and has been extensively investigated. The $\alpha_v\beta_3$ integrin binds to the arginine–glycine–aspartic acid (RGD) peptide sequence. Inhibition of this interaction with monoclonal antibodies or RGD antagonists induces cellular death and inhibits angiogenesis [61]. The RGD peptide can be labeled, for instance with ^{18}F, to synthesize a PET-capable integrin-targeted imaging agent of angiogenesis [54, 62–74] (Table 2). However, creating stable RGD peptides that can still hold an imaging label is challenging. Serum stability is an issue, and there can be confusion between uptake related to tumor expression and endothelial expression of $\alpha_v\beta_3$ integrin.

The MMPs are a family of zinc-dependent endogenous proteolytic enzymes that can selectively break down extracellular matrix and nonmatrix proteins. Tumors such as lung, colon, breast, and pancreas cancers typically secrete MMPs to remodel the surrounding microenvironment to promote new vessel formation [75]. The best-known MMPs are collagenase, stromelysins, metalloelastase, gelatinases, and membrane-type MMPs. Thus, MMPs are an excellent target for molecular imaging [76–79] (Table 3).

Targeted Imaging With Ultrasound

Targeted microbubble-enhanced sonography has been reported to be effective for both in vivo molecular imaging and quantification of VEGF receptor-2 and integrin. Microbubbles are formed that express the targeting ligand on their outer surface. VEGF receptor-2 expression was shown in human breast cancer and mice angiosarcoma tumor models by targeted microbubble-enhanced sonography [52–54]. For integrins, microbubbles labeled with peptides targeting the $\alpha_v\beta_3$ integrin were shown to provide noninvasive detection of angiogenic vessels in murine models of malignant gliomas [62]. Willmann et al. [54] reported improvement of in vivo visualization of tumor angiogenesis in a human ovarian cancer xenograft tumor model in mice by using dual-targeted microbubble-enhanced ultrasound directed at both VEGF receptor-2 and $\alpha_v\beta_3$ integrin. Targeted microbubbles have extraordinary sensitivity; only a few microbubbles are needed for detection. Such agents will probably be translated into clinical use in the near future. However, the

fundamental caveats of ultrasound still apply: limited field of view, difficulties in quantifying signal, and dependence on the expertise of the operator.

Targeted Imaging With MRI

Besides its anatomic and functional qualities for imaging of tumor angiogenesis, MRI has also been used for targeted imaging, especially for detection of $\alpha_v\beta_3$ integrin expression in tumors. Schmieder et al. [63] showed $\alpha_v\beta_3$ integrin expression in human melanoma murine tumor models by using $\alpha_v\beta_3$-targeted paramagnetic nanoparticles at 1.5 T, whereas Lee et al. [64] developed an iron oxide–based nanoprobe for simultaneous PET and MRI using a polyaspartic acid–coated iron oxide and showed integrin-dependent uptake in human glioblastoma murine tumor models. Despite the recent developments in targeted MRI of angiogenic molecules, it can be difficult to image the tumor neovasculature using MRI because vessels constitute only a small percentage of a tumor. Higher field strengths with newly designed coils and novel high-relaxivity molecular agents may allow better-targeted angiogenesis imaging with MRI.

Targeted Imaging With PET

PET, because of its superior sensitivity, has been the leading technique for targeted imaging of tumor angiogenesis. Extensive preclinical trials were performed for detecting the expression of angiogenesis molecules in tumors. For instance, Cai et al. [56] labeled a variant of VEGF, $VEGF_{121}$, with ^{64}Cu and showed in vivo uptake in mice with human glioblastoma xenografts correlating with VEGF receptor expression. Nagengast et al. [57] developed a form of bevacizumab that permitted both ^{111}In (for SPECT) and ^{89}Zr labeling (for PET) and found a high uptake of radiolabeled bevacizumab in the human SKOV-3 ovarian tumor xenograft. Recently, Wang et al. [58] developed a VEGF receptor-2–specific PET radiotracer, ^{64}Cu-DOTA (tetraazacyclodo-decanetetraacetic acid)-VEGF in a murine breast tumor model and showed tumor-specific uptake of this targeted agent. Targeted imaging of $\alpha_v\beta_3$ integrin has been widely studied. Haubner et al. [65] labeled RGD peptide with ^{18}F and showed a high and selective binding affinity for $\alpha_v\beta_3$ in melanoma and osteosarcoma tumor models in mice. Chen et al. [66] used ^{18}F-labeled RGD peptide in glioblastoma tumor models in mice and showed its tumor targeting efficacy. Beer et al. [67–69] evaluated the efficacy of ^{18}F-labeled RGD peptide in several tumor types (e.g., melanoma, sarcoma, renal cell cancer, non–small cell lung cancer) in clinical trials and concluded that targeted imaging of $\alpha_v\beta_3$ expression with ^{18}Flabeled RGD peptide correlates with $\alpha_v\beta_3$ expression at immunohistochemistry. Targeted PET was used for detecting the expression of MMPs by labeling MMP inhibitors with several radiotracers. However, results of in vivo imaging trials at PET using the MMPs as targeting moieties are not promising [76–78].

Optical Imaging

Optical imaging is a rapidly developing branch of medical imaging that does not require ionizing radiation exposure and can be acquired with relatively low cost and portable equipment. Optical imaging probes use fluorophores that first must be excited with a photon before they release a photon, typically of longer wavelength (lower energy) than the excitation light. Near-infrared fluorophores have the best tissue penetration and therefore are preferred for transcutaneous imaging. The major limitation of optical imaging as a whole-body imaging technique is its limited depth penetration; it is typically limited to several centimeters below the surface and even then only after considerable blurring due to light scattering. Therefore, optical imaging is reserved for superficial tissues or during endoscopy or surgery. Another limitation of optical imaging is autofluorescence, which is light emitted by endogenous and nonspecific exogenous molecules in the body. Among targeted agents developed for optical imaging of angiogenesis are Cy5.5-RGD peptides and the multivalent

Cy5.5-RAFT-cRGD peptides [72–74] (Fig. 7). Moreover, optical fluorophores can be combined with “smart probes” that are cleaved by MMPs to create activatable molecular imaging probes [79]. One concern is that optical fluorophores can have their own nonspecific tissue-binding characteristics that can influence the affinity of an optical molecular probe for nontargeted tissue. Clinical translation of optical agents and imaging needs further research on developing more sophisticated probes and translating them into the clinic.

Functional or Targeted Imaging?

Which of the two current strategies of imaging angiogenesis is preferred? The major advantage of functional techniques is that they are easily implemented with current technology and do not require regulatory approval for a new contrast media. The limitation is that they are relatively nonspecific for tumor angiogenesis and are only semiquantitative. The major advantage of targeted techniques is that they more precisely characterize the state of the endothelium in a tumor. The major disadvantage is that they require the synthesis of new compounds, which will require considerable time and resources to pass regulatory hurdles to enable human imaging. It is still unclear how important these agents will be in the future, but one suspects that as the economics of health care are more closely scrutinized, imaging could be used more commonly as a “gatekeeper” for patients to receive particular therapies. Moreover, the need for noninvasive biomarkers will mean that imaging will play a larger role in drug development. Even if such tests are expensive, they may eliminate the unwarranted use of even more expensive therapies. For this task, specific targeted imaging will likely be necessary.

Conclusion

Tumor angiogenesis is important for tumor growth and development. Current imaging techniques can be adapted to provide functional information regarding the status of the tumor vasculature. Future imaging will depend on the development of targeted imaging agents, probably PET- or SPECT-based, that will provide better specificity for angiogenic vessels and the early effects of molecular therapies. Therefore, the aim of imaging is shifting from functional to targeted molecular approaches. Although current experience with targeted molecular imaging is limited, further research in this field will eventually allow better characterization of tumor angiogenesis that will accelerate the development of targeted therapies for cancer.

Acknowledgments

Supported by the Intramural Research Program of the National Institutes of Health, National Cancer Institute, Center for Cancer Research.

References

1. Folkman J. Tumor angiogenesis: therapeutic implications. N Engl J Med. 1971; 18:1182–1186. [PubMed: 4938153]
2. Bergers G, Benjamin LE. Tumorigenesis and the angiogenic switch. Nat Rev Cancer. 2003; 3:401–410. [PubMed: 12778130]
3. Cosgrove D. Angiogenesis imaging: ultrasound. Br J Radiol. 2003; 76(spec no 1):S43–S49. [PubMed: 15456713]
4. Hata K, Nagami H, Iida K, Miyazaki K, Collins WP. Expression of thymidine phosphorylase in malignant ovarian tumors: correlation with microvessel density and an ultrasound-derived index of angiogenesis. Ultrasound Obstet Gynecol. 1998; 12:201–206. [PubMed: 9793193]

5. Yang WT, Tse GM, Lam PK, Metreweli C, Chang J. Correlation between color power Doppler sonographic measurement of breast tumor vasculature and immunohistochemical analysis of microvessel density for the quantitation of angiogenesis. J Ultrasound Med. 2002; 21:1227–1235. [PubMed: 12418764]
6. Alcázar JL. Tumor angiogenesis assessed by three-dimensional power Doppler ultrasound in early, advanced and metastatic ovarian cancer: a preliminary study. Ultrasound Obstet Gynecol. 2006; 28:325–329. [PubMed: 16906635]
7. Lagalla R, Caruso G, Urso R, Bizzini G, Marasà L, Miceli V. The correlations between color Doppler using a contrast medium and the neoangiogenesis of small prostatic carcinomas. Radiol Med (Torino). 2000; 99:270–275. [PubMed: 10884828]
8. D'Arcy TJ, Jayaram V, Lynch M, et al. Ovarian cancer detected non-invasively by contrast-enhanced power Doppler ultrasound. BJOG. 2004; 111:619–622. [PubMed: 15198792]
9. Hotta N, Tagaya T, Maeno T, et al. Advanced dynamic flow imaging with contrast-enhanced ultrasonography for the evaluation of tumor vascularity in liver tumors. Clin Imaging. 2005; 29:34–41. [PubMed: 15859016]
10. Lamuraglia M, Escudier B, Chami L, et al. To predict progression-free survival and overall survival in metastatic renal cancer treated with sorafenib: pilot study using dynamic contrast-enhanced Doppler ultrasound. Eur J Cancer. 2006; 42:2472–2479. [PubMed: 16965911]
11. Wang Z, Tang J, An L, et al. Contrast-enhanced ultrasonography for assessment of tumor vascularity in hepatocellular carcinoma. J Ultrasound Med. 2007; 26:757–762. [PubMed: 17526607]
12. Korpanty G, Carbon JG, Grayburn PA, Fleming JB, Brekken RA. Monitoring response to anticancer therapy by targeting microbubbles to tumor vasculature. Clin Cancer Res. 2007; 13:323–330. [PubMed: 17200371]
13. Nishida M, Koito K, Hirokawa N, Hori M, Satoh T, Hareyama M. Does contrast-enhanced ultrasound reveal tumor angiogenesis in pancreatic ductal carcinoma? A prospective study. Ultrasound Med Biol. 2009; 35:175–185. [PubMed: 18845377]
14. Balleyguier C, Opolon P, Mathieu MC, et al. New potential and applications of contrast-enhanced ultrasound of the breast: own investigations and review of the literature. Eur J Radiol. 2009; 69:14–23. [PubMed: 18977102]
15. Ma SH, Le HB, Jia BH, et al. Peripheral pulmonary nodules: relationship between multi-slice spiral CT perfusion imaging and tumor angiogenesis and VEGF expression. BMC Cancer. 2008; 8:186. [PubMed: 18590539]
16. Ippolito D, Sironi S, Pozzi M, et al. Hepatocellular carcinoma in cirrhotic liver disease: functional computed tomography with perfusion imaging in the assessment of tumor vascularization. Acad Radiol. 2008; 15:919–927. [PubMed: 18572129]
17. Sabir A, Schor-Bardach R, Wilcox CJ, et al. Perfusion MDCT enables early detection of therapeutic response to antiangiogenic therapy. AJR. 2008; 191:133–139. [PubMed: 18562736]
18. Li ZP, Meng QF, Sun CH, et al. Tumor angiogenesis and dynamic CT in colorectal carcinoma: radiologic– pathologic correlation. World J Gastroenterol. 2005; 11:1287–1291. [PubMed: 15761965]
19. Haider MA, Milosevic M, Fyles A, et al. Assessment of the tumor microenvironment in cervix cancer using dynamic contrast enhanced CT, interstitial fluid pressure and oxygen measurements. Int J Radiat Oncol Biol Phys. 2005; 62:1100–1107. [PubMed: 15990015]
20. Makari Y, Yasuda T, Doki Y, et al. Correlation between tumor blood flow assessed by perfusion CT and effect of neoadjuvant therapy in advanced esophageal cancers. J Surg Oncol. 2007; 96:220–229. [PubMed: 17450532]
21. Miles KA. Perfusion CT for the assessment of tumour vascularity: which protocol? Br J Radiol. 2003; 76:S36–S42. [PubMed: 15456712]
22. Choyke PL, Dwyer AJ, Knopp MV. Functional tumor imaging with dynamic contrast-enhanced magnetic resonance imaging. J Magn Reson Imaging. 2003; 17:509–520. [PubMed: 12720260]
23. Tofts PS, Brix G, Buckley DL, et al. Estimating kinetic parameters from dynamic contrast-enhanced T(1)-weighted MRI of a diffusable tracer: standardized quantities and symbols. J Magn Reson Imaging. 1999; 10:223–232. [PubMed: 10508281]

24. Liu PF, Krestin GP, Huch RA, Göhde SC, Caduff RF, Debatin JF. MRI of the uterus, uterine cervix, and vagina: diagnostic performance of dynamic contrast-enhanced fast multiplanar gradient-echo imaging in comparison with fast spin-echo T2- weighted pulse imaging. Eur Radiol. 1998; 8:1433–1440. [PubMed: 9853231]
25. Jager GJ, Ruijter ET, van de Kaa CA, et al. Dynamic turboFLASH subtraction technique for contrast-enhanced MR imaging of the prostate: correlation with histopathologic results. Radiology. 1997; 203:645–652. [PubMed: 9169683]
26. Hoskin PJ, Saunders MI, Goodchild K, Powell ME, Taylor NJ, Baddeley H. Dynamic contrast enhanced magnetic resonance scanning as a predictor of response to accelerated radiotherapy for advanced head and neck cancer. Br J Radiol. 1999; 72:1093–1098. [PubMed: 10700827]
27. Barentsz JO, Berger-Hartog O, Witjes JA, et al. Evaluation of chemotherapy in advanced urinary bladder cancer with fast dynamic contrast-enhanced MR imaging. Radiology. 1998; 207:791–797. [PubMed: 9609906]
28. Reddick WE, Taylor JS, Fletcher BD. Dynamic MR imaging (DEMRI) of microcirculation in bone sarcoma. J Magn Reson Imaging. 1999; 10:277–285. [PubMed: 10508287]
29. Devries AF, Griebel J, Kremser C, et al. Tumor microcirculation evaluated by dynamic magnetic resonance imaging predicts therapy outcome for primary rectal carcinoma. Cancer Res. 2001; 61:2513–2516. [PubMed: 11289123]
30. Hayes C, Padhani AR, Leach MO. Assessing changes in tumour vascular function using dynamic contrast-enhanced magnetic resonance imaging. NMR Biomed. 2002; 15:154–163. [PubMed: 11870911]
31. Mayr NA, Yuh WT, Arnholt JC, et al. Pixel analysis of MR perfusion imaging in predicting radiation therapy outcome in cervical cancer. J Magn Reson Imaging. 2000; 12:1027–1033. [PubMed: 11105046]
32. Thukral A, Thomasson DM, Chow CK, et al. Inflammatory breast cancer: dynamic contrast-enhanced MR in patients receiving bevacizumab— initial experience. Radiology. 2007; 244:727–735. [PubMed: 17709827]
33. Wedam SB, Low JA, Yang SX, et al. Antiangiogenic and antitumor effects of bevacizumab in patients with inflammatory and locally advanced breast cancer. J Clin Oncol. 2006; 24:769–777. [PubMed: 16391297]
34. Ocak I, Bernardo M, Metzger G, et al. Dynamic contrast-enhanced MRI of prostate cancer at 3 T: a study of pharmacokinetic parameters. AJR. 2007; 189:849. [web]W192–W201. [PubMed: 17885055]
35. Kosaka N, Uematsu H, Kimura H, et al. Assessment of the vascularity of uterine leiomyomas using double-echo dynamic perfusion-weighted MRI with the first-pass pharmacokinetic model: correlation with histopathology. Invest Radiol. 2007; 42:629–635. [PubMed: 17700278]
36. Preda A, Novikov V, Möglich M, et al. MRI monitoring of Avastin antiangiogenesis therapy using B22956/1, a new blood pool contrast agent, in an experimental model of human cancer. J Magn Reson Imaging. 2004; 20:865–873. [PubMed: 15503324]
37. Marzola P, Degrassi A, Calderan L, et al. Early antiangiogenic activity of SU11248 evaluated in vivo by dynamic contrast-enhanced magnetic resonance imaging in an experimental model of colon carcinoma. Clin Cancer Res. 2005; 11:5827–5832. [PubMed: 16115922]
38. Taylor, NJ.; Lankester, KJ.; Stirling, JJ., et al. Application, of navigator techniques to breath-hold DCE-MRI studies of the liver. Proceedings of the International Society of Magnetic Resonance in Medicine 11th scientific meeting; Berkeley, CA: ISMRM; 2003. p. 1306
39. Castro, MA.; Yao, J.; Turkbey, B.; Pang, Y.; Choyke, PL.; Thomasson, D. Improvement of DCE-MRI images to study liver cancer by means of a deformable registration algorithm. (abstr). Proceedings of the annual meeting of the Radiological Society of North America (RSNA); Chicago, IL: RSNA; 2008. p. 691
40. Anderson H, Yap JT, Wells P, et al. Measurement of renal tumour and normal tissue perfusion using positron emission tomography in a phase II clinical trial of razoxane. Br J Cancer. 2003; 89:262–267. [PubMed: 12865914]

41. Wells P, Jones T, Price P. Assessment of inter- and intrapatient variability in C15O2 positron emission tomography measurements of blood flow in patients with intra-abdominal cancers. Clin Cancer Res. 2003; 9:6350–6356. [PubMed: 14695134]
42. Hentschel M, Paulus T, Mix M, Moser E, Nitzsche EU, Brink I. Analysis of blood flow and glucose metabolism in mammary carcinomas and normal breast: a H_2(15)O PET and ^{18}F-FDG PET study. Nucl Med Commun. 2007; 28:789–797. [PubMed: 17728609]
43. Longo R, Gasparini G. Anti-VEGF therapy: the search for clinical biomarkers. Expert Rev Mol Diagn. 2008; 8:301–314. [PubMed: 18598109]
44. Cho SM, Park YG, Lee JM, et al. ^{18}F-fluorodeoxyglucose positron emission tomography in patients with recurrent ovarian cancer: in comparison with vascularity, Ki-67, p53, and histologic grade. Eur Radiol. 2007; 17:409–417. [PubMed: 16786320]
45. Bos R, van Der Hoeven JJ, van Der Wall E, et al. Biologic correlates of (18)fluorodeoxyglucose uptake in human breast cancer measured by positron emission tomography. J Clin Oncol. 2002; 20:379–387. [PubMed: 11786564]
46. Zasadny KR, Tatsumi M, Wahl RL. FDG metabolism and uptake versus blood flow in women with untreated primary breast cancers. Eur J Nucl Med Mol Imaging. 2003; 30:274–280. [PubMed: 12552346]
47. Guo J, Higashi K, Ueda Y, et al. Microvessel density: correlation with ^{18}F-FDG uptake and prognostic impact in lung adenocarcinomas. J Nucl Med. 2006; 47:419–425. [PubMed: 16513610]
48. Buck AK, Reske SN. Cellular origin and molecular mechanisms of ^{18}F-FDG uptake: is there a contribution of the endothelium? J Nucl Med. 2004; 45:461–463. [PubMed: 15001688]
49. Ferrara N. Vascular endothelial growth factor: basic science and clinical progress. Endocr Rev. 2004; 25:581–611. [PubMed: 15294883]
50. Kowanetz M, Ferrara N. Vascular endothelial growth factor signaling pathways: therapeutic perspective. Clin Cancer Res. 2006; 12:5018– 5022. [PubMed: 16951216]
51. Middleton G, Lapka DV. Bevacizumab (Avastin). Clin J Oncol Nurs. 2004; 8:666–669. [PubMed: 15637962]
52. Lyshchik A, Fleischer AC, Huamani J, Hallahan DE, Brissova M, Gore JC. Molecular imaging of vascular endothelial growth factor receptor 2 expression using targeted contrast-enhanced highfrequency ultrasonography. J Ultrasound Med. 2007; 26:1575–1586. [PubMed: 17957052]
53. Lee DJ, Lyshchik A, Huamani J, Hallahan DE, Fleischer AC. Relationship between retention of a vascular endothelial growth factor receptor 2 (VEGFR2)-targeted ultrasonographic contrast agent and the level of VEGFR2 expression in an in vivo breast cancer model. J Ultrasound Med. 2008; 27:855–866. [PubMed: 18499845]
54. Willmann JK, Paulmurugan R, Chen K, et al. US imaging of tumor angiogenesis with microbubbles targeted to vascular endothelial growth factor receptor type 2 in mice. Radiology. 2008; 246:508–518. [PubMed: 18180339]
55. Hsu AR, Cai W, Veeravagu A, et al. Multi-modality molecular imaging of glioblastoma growth inhibition with vasculature-targeting fusion toxin VEGF121/rGel. J Nucl Med. 2007; 48:445–454. [PubMed: 17332623]
56. Cai W, Chen K, Mohamedali KA, et al. PET of vascular endothelial growth factor receptor expression. J Nucl Med. 2006; 47:2048–2056. [PubMed: 17138749]
57. Nagengast WB, de Vries EG, Hospers GA, et al. In vivo VEGF imaging with radiolabeled bevacizumab in a human ovarian tumor xenograft. J Nucl Med. 2007; 48:1313–1319. [PubMed: 17631557]
58. Wang H, Cai W, Chen K, et al. A new PET tracer specific for vascular endothelial growth factor receptor 2. Eur J Nucl Med Mol Imaging. 2007; 34:2001–2010. [PubMed: 17694307]
59. Backer MV, Gaynutdinov TI, Patel V, et al. Vascular endothelial growth factor selectively targets boronated dendrimers to tumor vasculature. Mol Cancer Ther. 2005; 4:1423–1429. [PubMed: 16170035]
60. Ruoslahti E. Specialization of tumour vasculature. Nat Rev Cancer. 2002; 2:83–90. [PubMed: 12635171]
61. Cai W, Chen X. Anti-angiogenic cancer therapy based on integrin alphavbeta$_3$ antagonism. Anticancer Agents Med Chem. 2006; 6:407–428. [PubMed: 17017851]

62. Ellegala DB, Leong-Poi H, Carpenter JE, et al. Imaging tumor angiogenesis with contrast ultrasound and microbubbles targeted to alpha(v)beta$_3$. Circulation. 2003; 108:336–341. [PubMed: 12835208]
63. Schmieder AH, Winter PM, Caruthers SD, et al. Molecular MR imaging of melanoma angiogenesis with alphanubeta$_3$-targeted paramagnetic nanoparticles. Magn Reson Med. 2005; 53:621–627. [PubMed: 15723405]
64. Lee HY, Li Z, Chen K, et al. PET/MRI dual-modality tumor imaging using arginine-glycine-aspartic (RGD)-conjugated radiolabeled iron oxide nanoparticles. J Nucl Med. 2008; 49:1371–1379. [PubMed: 18632815]
65. Haubner R, Wester HJ, Weber WA, et al. Noninvasive imaging of alpha(v)beta$_3$ integrin expression using ^{18}F-labeled RGD-containing glycopeptide and positron emission tomography. Cancer Res. 2001; 61:1781–1785. [PubMed: 11280722]
66. Chen X, Park R, Shahinian AH, et al. ^{18}F-labeled RGD peptide: initial evaluation for imaging brain tumor angiogenesis. Nucl Med Biol. 2004; 31:179– 189. [PubMed: 15013483]
67. Beer AJ, Haubner R, Goebel M, et al. Biodistribution and pharmacokinetics of the alpha$_v$beta$_3$-selective tracer ^{18}F-galacto-RGD in cancer patients. J Nucl Med. 2005; 46:1333–1341. [PubMed: 16085591]
68. Beer AJ, Haubner R, Sarbia M, et al. Positron emission tomography using [^{18}F]Galacto-RGD identifies the level of integrin alpha(v)beta$_3$ expression in man. Clin Cancer Res. 2006; 12:3942–3949. [PubMed: 16818691]
69. Beer AJ, Lorenzen S, Metz S, et al. Comparison of integrin alpha$_v$beta$_3$ expression and glucose metabolism in primary and metastatic lesions in cancer patients: a PET study using ^{18}F-galacto-RGD and ^{18}F-FDG. J Nucl Med. 2008; 49:22–29. [PubMed: 18077538]
70. Kenny LM, Coombes RC, Oulie I, et al. Phase I trial of the positron-emitting Arg-Gly-Asp (RGD) peptide radioligand ^{18}F-AH111585 in breast cancer patients. J Nucl Med. 2008; 49:879–886. [PubMed: 18483090]
71. Decristoforo C, Hernandez Gonzalez I, Carlson J, et al. (68)Ga- and (111)In-labeled DOTA-RGD peptides for imaging of alpha$_v$beta$_3$ integrin expression. Eur J Nucl Med Mol Imaging. 2008; 35:1507–1515. [PubMed: 18369617]
72. Chen X, Conti PS, Moats RA. In vivo near-infrared fluorescence imaging of integrin alpha$_v$beta$_3$ in brain tumor xenografts. Cancer Res. 2004; 64:8009–8014. [PubMed: 15520209]
73. Jin ZH, Josserand V, Foillard S, et al. In vivo optical imaging of integrin alpha$_v$-beta$_3$ in mice using multivalent or monovalent cRGD targeting vectors. Mol Cancer. 2007; 6:41. [PubMed: 17565663]
74. Hsu AR, Hou LC, Veeravagu A, et al. In vivo near-infrared fluorescence imaging of integrin alpha$_v$beta$_3$ in an orthotopic glioblastoma model. Mol Imaging Biol. 2006; 8:315–323. [PubMed: 17053862]
75. Li WP, Anderson CJ. Imaging matrix metalloproteinase expression in tumors. Q J Nucl Med. 2003; 47:201–208. [PubMed: 12897711]
76. Furumoto S, Takashima K, Kubota K, Ido T, Iwata R, Fukuda H. Tumor detection using ^{18}F-labeled matrix metalloproteinase-2 inhibitor. Nucl Med Biol. 2003; 30:119–125. [PubMed: 12623110]
77. Medina OP, Kairemo K, Valtanen H, et al. Radio-nuclide imaging of tumor xenografts in mice using a gelatinase-targeting peptide. Anticancer Res. 2005; 25:33–42. [PubMed: 15816516]
78. Zheng QH, Fei X, Liu X, et al. Comparative studies of potential cancer biomarkers carbon-11 labeled MMP inhibitors (S)-2-(4′-[^{11}C]methoxybiphenyl- 4-sulfonylamino)-3-methylbutyric acid and N-hydroxy-(R)-2-[[(4′-[^{11}C]methoxyphenyl) sulfonyl]benzylamino]-3-methylbutanamide. Nucl Med Biol. 2004; 31:77–85. [PubMed: 14741572]
79. Bremer C, Bredow S, Mahmood U, Weissleder R, Tung CH. Optical imaging of matrix metalloproteinase- 2 activity in tumors: feasibility study in a mouse model. Radiology. 2001; 221:523–529. [PubMed: 11687699]
80. Liu Y, Bellomi M, Gatti G, Ping X. Accuracy of computed tomography perfusion in assessing metastatic involvement of enlarged axillary lymph nodes in patients with breast cancer. Breast Cancer Res. 2007; 9:R40. [PubMed: 17615058]

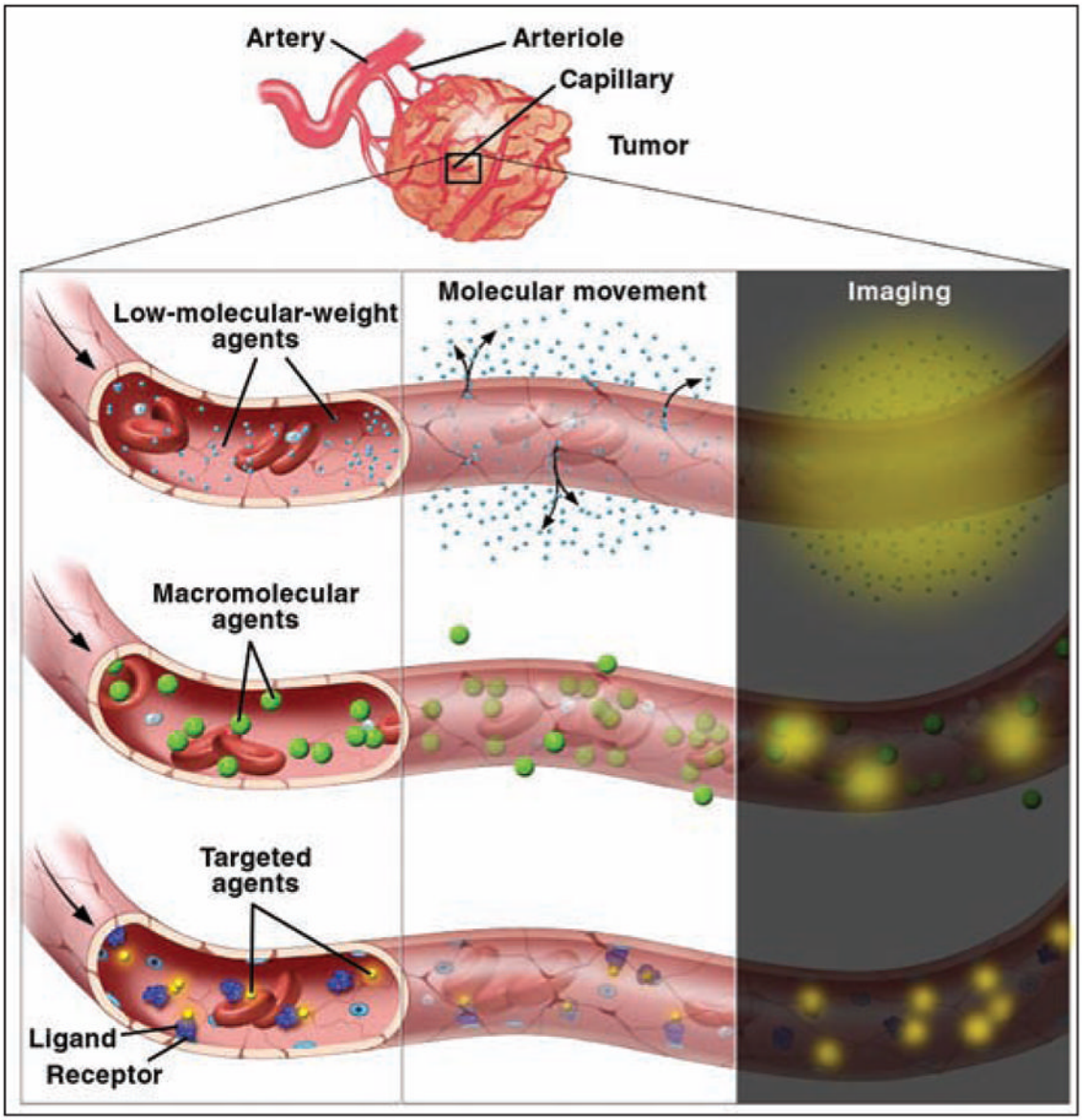

Fig. 1.
Illustration of low-molecular-weight, macromolecular, and targeted contrast agents diffusing from tumor vessels into interstitial space. Courtesy of Lydia V. Kibiuk, NIH/DMA.

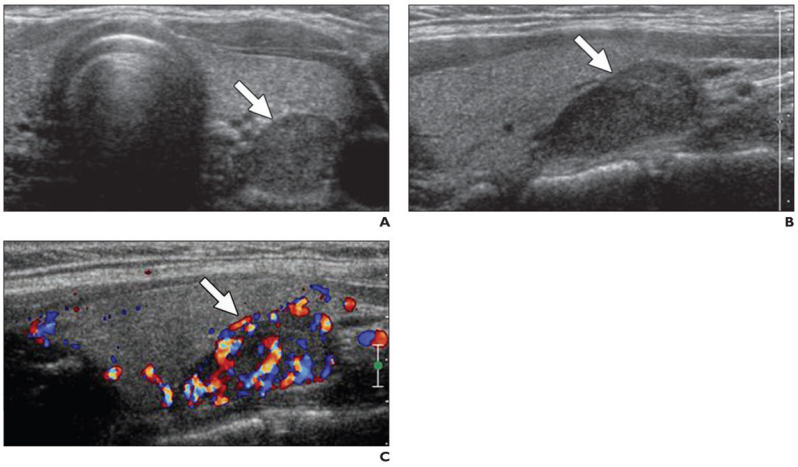

Fig. 2. 36-year-old woman with hypertension

A, Axial gray-scale ultrasound image obtained with conventional probe shows hypoechoic lesion at left inferior thyroid bed (*arrow*).

B, Sagittal gray-scale ultrasound image with high-resolution probe confirms presence of lesion (*arrow*).

C, Lesion shows increased vascularity at color Doppler mode, consistent with parathyroid adenoma (*arrow*).

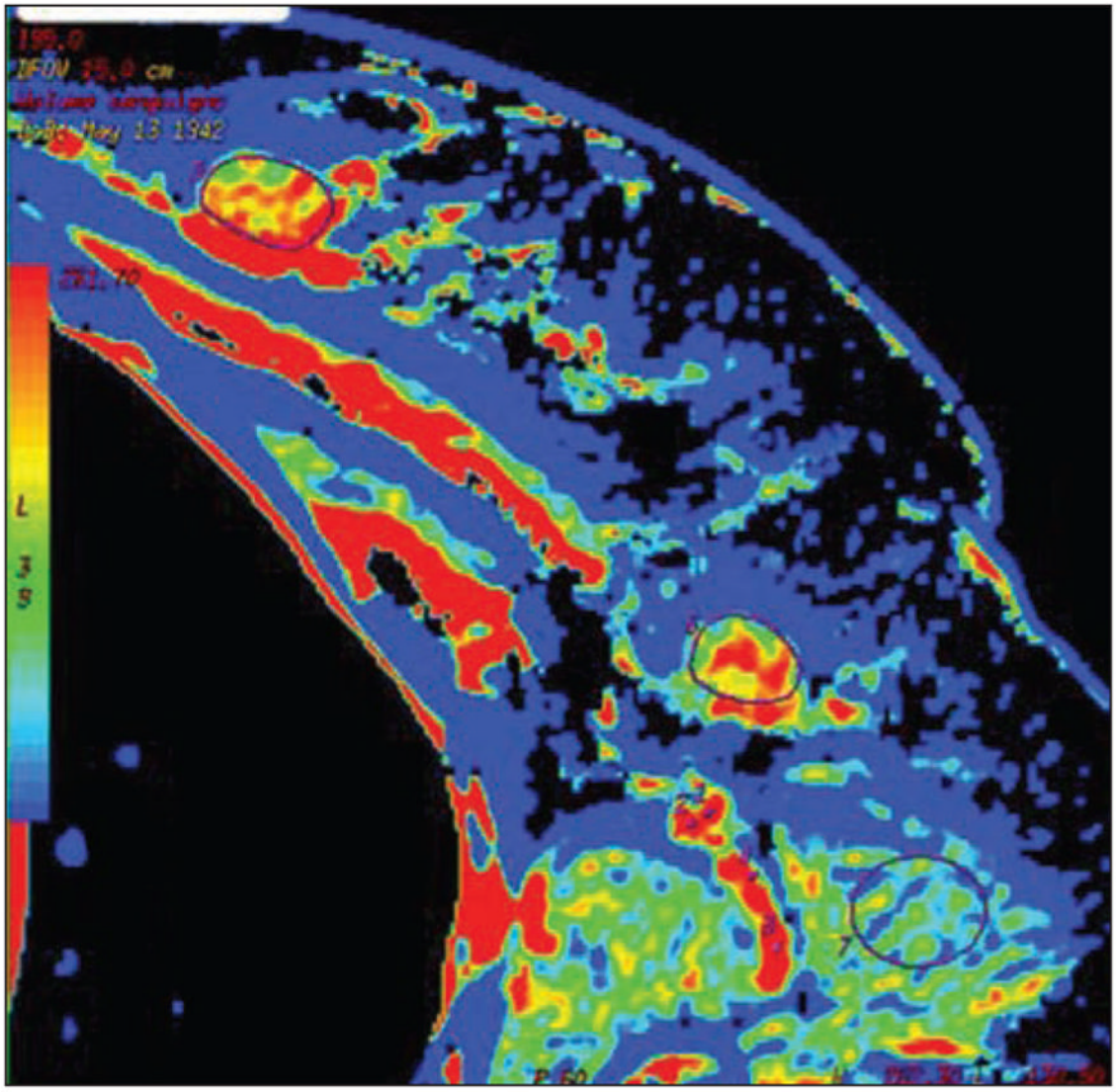

Fig. 3.

Colored map of blood volume obtained by CT perfusion in female patient with breast cancer and ipsilateral palpable node. Both primary tumor (outlined by region of interest [ROI]) and target node (outlined by ROI) are visible on this slice. High values of blood volume are depicted both in primary tumor and in target node. At postsurgical pathology, lymph node was determined to be metastatic. (Reprinted with permission from Liu Y, Bellomi M, Gatti G, Ping X. Accuracy of computed tomography perfusion in assessing metastatic involvement of enlarged axillary lymph nodes in patients with breast cancer. *Breast Cancer Res* 2007; 9:R40 [80])

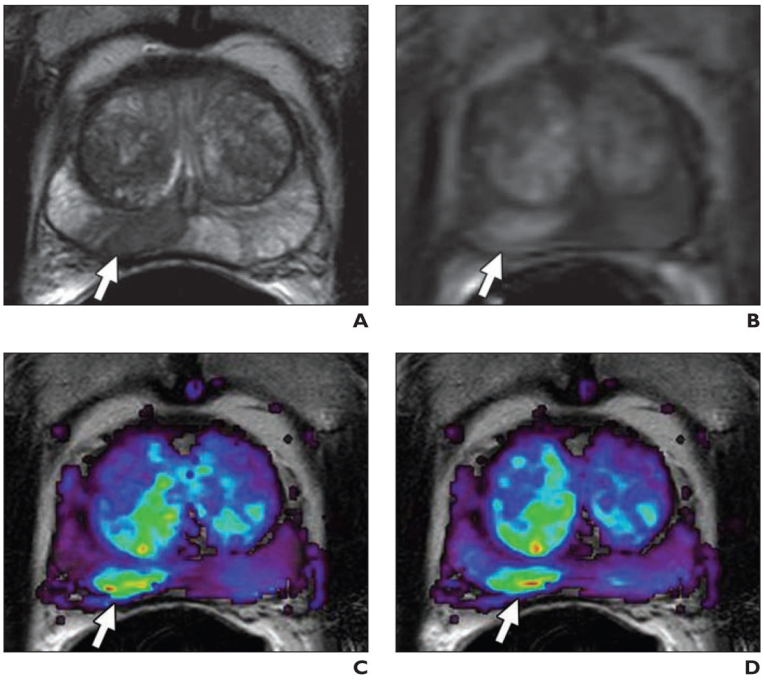

Fig. 4. 59-year-old man with prostate cancer

A, Axial T2-weighted MR image shows low-signal-intensity foci suspicious for prostate cancer at right mid peripheral zone (*arrow*).

B, Raw dynamic contrast-enhanced MR image shows significant enhancement of lesion (*arrow*).

C and **D,** Corresponding K^{trans} (transendothelial transport of contrast medium from vascular compartment to the tumor interstitium) (**C**) and k_{ep} (reverse transport parameter of contrast medium back into the vascular space) (**D**) maps localize right peripheral zone tumor (*arrows*).

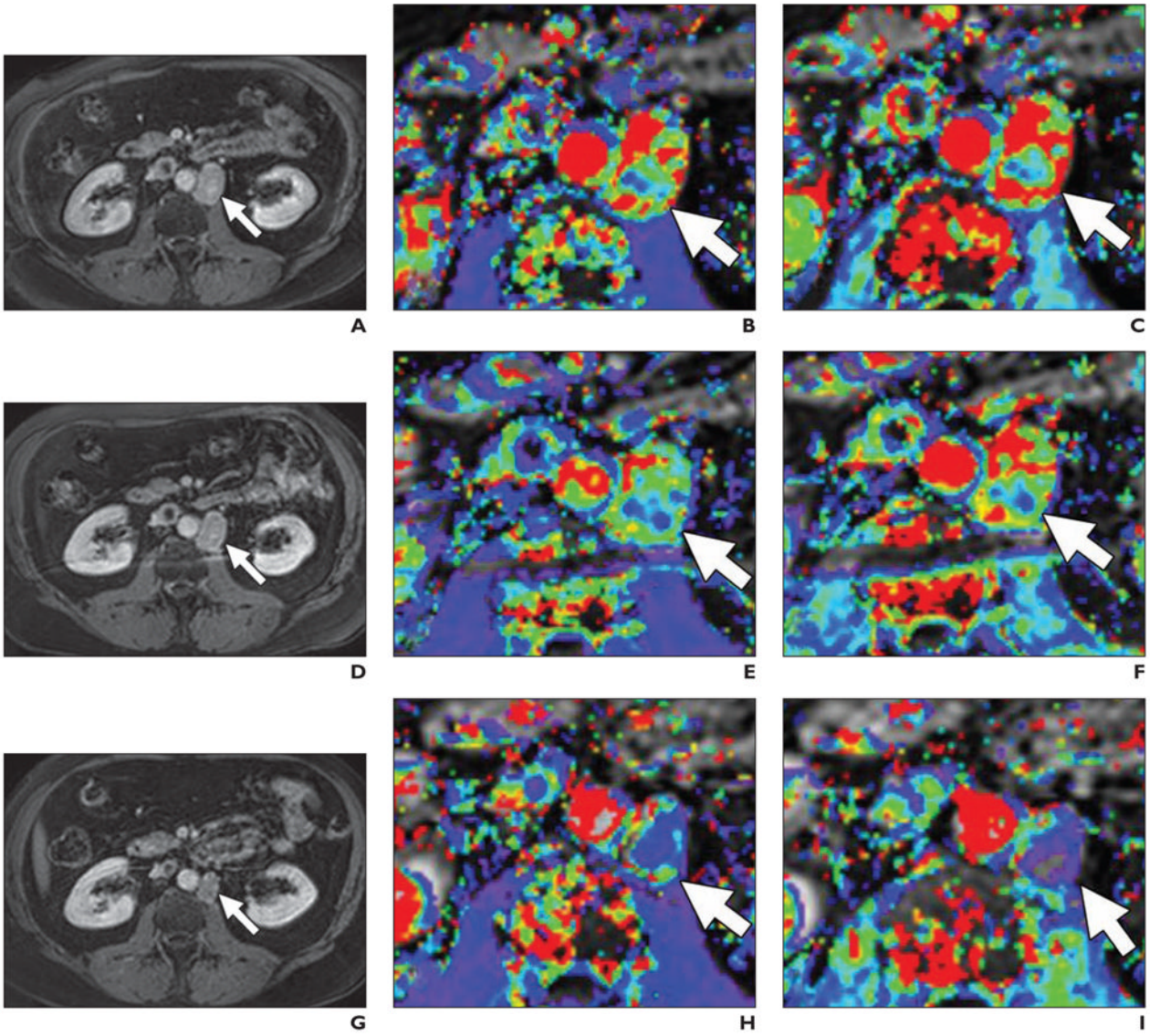

Fig. 5. 58-year-old man with metastatic prostate cancer

A–I, T1-weighted delayed contrast-enhanced MR images (**A, D,** and **G**), magnified K^{trans} (transendothelial transport of contrast medium from vascular compartment to the tumor interstitium) maps (**B, E, H**), and k_{ep} (reverse transport parameter of contrast medium back into the vascular space) maps (**C, F,** and **I**) before (*top row*), 24 hours after (*middle row*), and 1 month after (*bottom row*) antiangiogenesis therapy. K^{trans} and k_{ep} reductions are seen in retroperitoneal lymph node (*arrows*) despite relatively little change in node size.

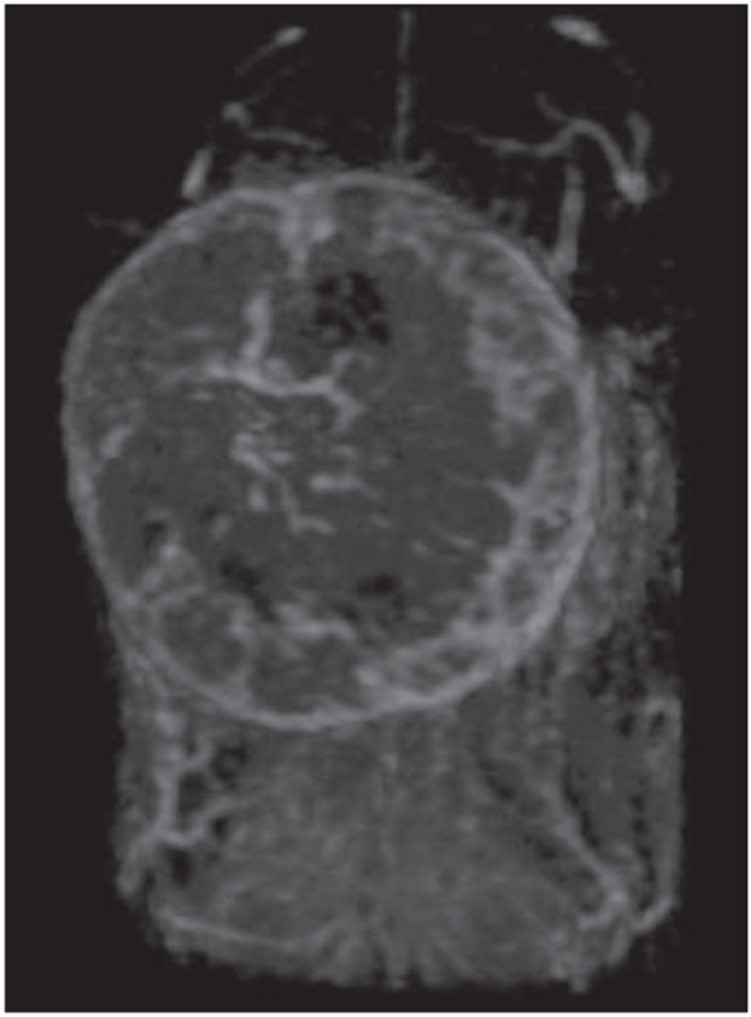

Fig. 6.
Three-dimensional dynamic contrast-enhanced MR image of orthotopically implanted breast cancer model produced with TUBO mice mammary breast cancer cell lines obtained 5 minutes after injection of 0.03 mmol Gd/kg of G6 (generation 6) dendrimer contrast agent via tail vein. Maximum-intensity- projection image cropped at site of breast tumor shows vascularity of tumor.

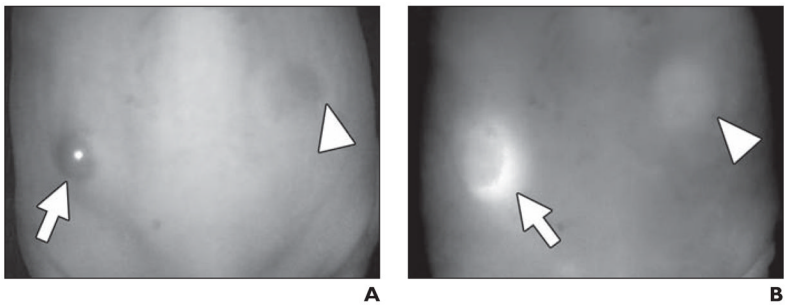

Fig. 7.

In vivo spectral fluorescence images obtained 4 days after injection of nonspecific blood pool agent, polyclonal IgG-Cy5.5 (50 μg, IV) into ATAC4 (left dorsum) (*arrow*) and A431 (right dorsum) (*arrowhead*) tumors in mice.

A (white light image) and **B** (Cy5.5 fluorescence image), IgG-Cy5.5 similarly accumulated in both tumors and also showed mouse body because of blood pool.

TABLE 1

Targeted VEGF and VEGF Receptor Imaging Studies in the Literature

Study Group, Year	Imaging Technique	Tumor Model	Contrast Agent and Label Used	Reference
Lyshcik et al., 2007	Ultrasound	Breast cancer in mice	VEGF receptor-2–targeted ultrasound contrast agent	52
Lee et al., 2008	Ultrasound	Breast cancer in mice	VEGF receptor-2–targeted ultrasound contrast agent	53
Willmann et al., 2008	Ultrasound	Angiosarcoma in mice	VEGF receptor-2–targeted ultrasound contrast agent	54
Hsu et al., 2007	PET	Glioblastoma in mice	^{64}Cu-DOTA-VEGF$_{121}$	55
Cai et al., 2006	PET	Glioblastoma in mice	^{64}Cu-labeled VEGF$_{121}$	56
Nagengast et al., 2007	SPECT and PET	SKOV-3 ovarian tumor xenograft in mice	^{111}In (SPECT), ^{89}Zr (PET)	57
Wang et al., 2007	PET	Murine breast cancer in mice	^{64}Cu-DOTA-VEGF (DEE)	58
Backer et al., 2005	Near-infrared fluorescence imaging	Breast cancer in mice	5th-generation dendrimer tagged with near-infrared Cy5	59

Note—VEGF = vascular endothelial growth factor, DOTA = tetraazacyclododecanetetraacetic acid.

TABLE 2

Targeted Integrin Imaging Studies in the Literature

Study Group, Year	Imaging Technique	Tumor Model	Contrast Agent and Label Used	Reference
Ellegala et al., 2003	Ultrasound	Malignant glioma in rats	Echistatin conjugated ultrasound contrast agent	62
Willmann et al., 2008	Ultrasound	Angiosarcoma in mice	α(v)β(3)-targeted ultrasound contrast agent	54
Scmieder et al., 2005	MRI	Human melanoma xenograft in mice	α(v)β(3)-targeted paramagnetic nano-particles	63
Lee et al., 2008	MRI and PET	Human glioblastoma in mice	Polyaspartic acid-coated iron oxide and ^{64}Cu	64
Haubner et al., 2001	PET	Murine osteosarcoma, human melanoma in mice	^{18}F-labeled RGD	65
Chen et al., 2004	PET	Glioblastoma in mice	^{18}F-labeled RGD	66
Beer et al., 2005	PET	Melanoma, sarcoma, or osseous metastases in 19 patients	^{18}F-labeled RGD	67
Beer et al., 2006	PET	Solid tumors (melonama, musculoskeletal tumors, etc.) in 19 patients	^{18}F-labeled RGD	68
Beer et al., 2008	PET	Various solid tumor types in human	^{18}F-labeled RGD	69
Kenny et al., 2008	PET	Breast cancer in human	^{18}F-AH111585-labeled RGD	70
Decristoforo et al., 2008	PET and SPECT	Melanoma in mice	^{68}Ga- and ^{111}In-labeled DOTA-RGD	71
Chen et al., 2004	Near-infrared fluorescence imaging	Glioblastoma in mice	Cy5.5-RGD	72
Jin et al., 2007	Near-infrared fluorescence imaging	Human embryonic kidney cells in mice	Cy5-RAFT-c(-RGDfK-) 4 (a tetrameric cRGD)	73
Hsu et al., 2006	Near-infrared fluorescence imaging	Glioblastoma in mice	Cy5.5-RGD	74

Note—RGD = arginine–glycine–aspartic acid, DOTA = tetraazacyclododecanetetraacetic acid.

TABLE 3

Targeted Matrix Metalloproteinase (MMP) Imaging Studies in the Literature

Study Group, Year	Imaging Technique	Tumor Model	Contrast Agent and Label Used	Reference
Furumoto et al., 2003	PET	Breast cancer in mice	^{18}F-labeled MMP	76
Medina et al., 2005	SPECT	Xenograft tumor in mice	^{125}I- and ^{99m}Tc-labeled gelatinase inhibitory peptide	77
Zheng et al., 2004	PET	Breast cancer in mice	^{11}C-labeled MMP inhibitors	78
Bremer et al., 2001	Near-infrared fluorescence imaging	Human fibrosarcoma in mice	Optical fluorophores	79